metals

MDPI

Article

Influence of Friction Coefficient on the Performance of Cold Forming Tools

Eneko Barba [1,2,*], Daniel Salcedo [1], Adrian Claver [1], Rodrigo Luri [1] and Jose A. Garcia [1]

[1] Engineering Department, Public University of Navarre (UPNA), Campus Arrosadía S/N, 31006 Pamplona, Spain; daniel.salcedo@unavarra.es (D.S.); adrian.claver@unavarra.es (A.C.); rodrigo.luri@unavarra.es (R.L.); joseantonio.garcia@unavarra.es (J.A.G.)
[2] NUADI, Polígono Ind. Arazuri-Orcoyen, Calle D, 2, 31170 Arazuri, Spain
* Correspondence: eneko.barba@nuadi.com; Tel.: +34-948-281090

Abstract: The automotive industry has undergone significant advancements and changes over time, resulting in the use of more complex parts in modern vehicles. As a consequence, the parts used in the manufacturing process are subject to higher stress levels, which reduce their service life. To mitigate this issue, surface treatments can be applied to improve the mechanical properties of the tools. In this study, we examined the impact of surface treatments on reducing tool stress during a cold forming process. The process involved reducing the thickness of a sheet from 6 mm to 2.5 mm, which generated high stresses in the tooling. We used finite element stress calculations to analyze the process and found that by reducing the friction coefficient to 0.1, tool stresses can be reduced by 20%, leading to an increase in tool life. Moreover, the press force and tool wear were also reduced by 18%. To validate the theoretical calculations, we performed field tests in a real manufacturing process.

Keywords: forming; finite element method; friction coefficient; coatings; wear

Citation: Barba, E.; Salcedo, D.; Claver, A.; Luri, R.; Garcia, J.A. Influence of Friction Coefficient on the Performance of Cold Forming Tools. *Metals* **2023**, *13*, 960. https://doi.org/10.3390/met13050960

Academic Editors: Andrzej Gontarz and Grzegorz Winiarski

Received: 7 April 2023
Revised: 11 May 2023
Accepted: 12 May 2023
Published: 15 May 2023

1. Introduction

One of the most important industrial sectors today is the automotive industry. It generates a business volume that represents 7% of the GDP of the European continent and employs almost 14 million people directly and indirectly, which represents 6.1% of total employment. Only 2.6 million people work in the production chain. Approximately 20% of the components of a car are manufactured by some type of forming process. This type of process has become more and more important and has replaced slower and more expensive manufacturing processes such as die casting. Stamping is a fast and reliable manufacturing process, capable of producing complex and resistant parts. Because of that, it has been chosen by many companies to manufacture their products [1].

The automotive industry lives in a continuous improvement process, it is one of the most competitive industries, and because of the quantities of production, a small improvement could make a huge impact on productivity. This has led to an increase in complexity of the parts used in modern vehicles, which reflects the intricate nature of the advanced automotive technology available today. However, this makes forming much more difficult and complex. As a result, an increase in stress on tools during the forming processes has been found [2]. The stress directly affects the tool behavior, where the wear or unexpected break could appear [3]. These failures result in higher production costs; therefore, new tools must be manufactured to replace the damaged ones, with the extra cost that this entails. Furthermore, press machine downtimes also directly affect the manufacturing costs. In addition, the issues derived from not satisfying the quality requirements demanded by the customer must be addressed. In some cases, even reprocessing work is needed.

Cold forming tools can face various performance issues during the manufacturing process. Some of the common issues include wear, cracking, chipping, and deformation of the tool material. These issues can arise due to various factors such as high contact stresses,

repetitive loading cycles, friction, and inadequate cooling. To address these issues, tool materials are selected based on their ability to withstand high stress and wear resistance. One area of focus is the study of new geometries for the tools, such as in the case of fine blanking [4], where a new die design was investigated regarding trying to reduce the die roll size. In this process, the geometry of the matrix was being carefully examined and modified to achieve better results. The objective was to create a tool that can produce high-precision, burr-free parts with excellent surface finish and dimensional accuracy. By exploring new geometries for the tooling, researchers hoped to achieve significant improvements in the efficiency, precision, and overall performance of the cold forming process. Similar to those two studies, the objective was to enhance the surface quality of the fracture generated by fine blanking [5,6].

In this way, the stamping industry has utilized surface treatments on tools with the objective of reducing stress, and consequently, extending tool life. Surface treatments change the mechanical properties of the tools, and that is why numerous researchers have delved into this field and reported their findings on how the surface finish of a tool impacts its wear development. Wu et al. studied the influence of the tool finishing on the wear development and the tool life [7]. Grouche et al. [8] demonstrated the influence of these two aspects, including the significance of tool roughness in this regard, while emphasizing the need to consider factors such as gliding speed and contact pressure [9]. Additionally, some authors have explored and created models for the relationship between load and wear [10]; this reference proposes a new testing method which allows for a high resolution of wear formation in time. In addition, one of the most involved properties is the friction coefficient, which is largely responsible for the tool performance. Reference [11] evaluated different surface modification techniques in terms of friction properties. To this end, how the reduction of friction directly affects the stresses received by tools was studied [12]. Brathikan et al. [13] related the friction and the blank diameter with the forming force.

Friction is critical in cold forming as it impacts the forces, energy, and surface quality of the product [14]. Different friction models used in cold forming include the Coulomb friction model, Amonton's friction model, Tresca friction model, and Tabor's friction model. The Coulomb model assumes that friction is proportional to the normal force [15], while Amonton's model adds a coefficient of friction. Tresca's model is based on the maximum shear stress and considers the frictional force proportional to the shear strength and contact area [16,17]. Tabor's model adds adhesion forces to the shear forces and is relevant for high surface roughness and pressure situations. The shear friction model in cold forming combines friction and shear deformation effects [18,19]. It considers the frictional force, proportional to the normal force and coefficient of friction, and the shear stress induced by deformation, proportional to the material's shear strength and strain rate, and influenced by the temperature and strain rate. The model predicts the deformation behavior and energy requirements for cold forming with high levels of shear deformation and optimizes process parameters for better mechanical properties and surface quality.

In this work, the forming process of some elements of the brake backing plate has been analyzed. The stresses received by the tools have been calculated and simulations have been effectuated using finite volume calculations, varying the friction coefficient, and using the shear model. The simulation software SIMUFACT FORMING has been used to study the stress. Different tests were also carried out in the laboratory to define the necessary parameters required by the software. The simulations were performed with two different friction coefficients, and it was possible to observe their effect on the load received by the tool.

In addition, to validate the results obtained in the simulations, field tests have been performed with the tools under study. These tools have been tested in the real manufacturing process. To test the same tools with different friction coefficients, an industrial PVD (physical vapor deposition) coating of DLC (diamond-like carbon) was used for its excellent tribological properties (friction coefficient < 0.1). Sulaiman et al. [20] analyzed the effects of DLC/TiAlN-coated die on friction and wear in sheet metal forming. These coatings offer friction coefficients around 0.1 and have already been studied for similar applications

in previous works [21,22] with positive results in tool steels. Although DLC coatings are known for their excellent tribological properties, they used to have an inadequate adhesion to the substrate. This fact made their implementation in stamping processes difficult. A few years ago, the HIPIMS [23] technique significantly improved their adhesion properties [24] and the deposition rate [25]. In addition, the novel technique of using positive pulses in the PVD discharge process [26] has made the adhesion good enough to be tested in industrial processes. Because of all this, DLC coatings were used to reduce the friction coefficient of die components in this study.

In conclusion, the study provides valuable insights into the impact of the friction coefficient on the cold forming tool life and highlights the effectiveness of using a finite element forming process simulation to study tool stresses. The findings of this research can be used by manufacturers and engineers to optimize tool selection and design, leading to improved performance and cost savings.

2. Simulation Model

2.1. Geometry

To fulfil the study, the forming process of a brake backing plate was analyzed Figure 1. This stamping process forms a shape called a straight chamfer. It is a particularly demanding forming process due to the reduction of the sheet thickness (6 mm) by more than 50%. Consequently, the stresses generated in the tool during the stamping process are exceptionally high, which can cause tool failures.

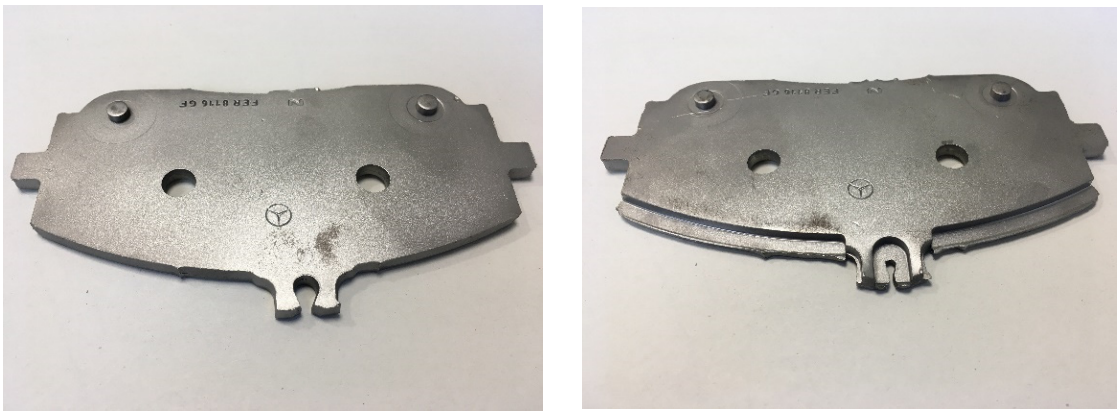

(**a**) (**b**)

Figure 1. Real part. (**a**) Before forming; (**b**) after forming.

To carry out the forming process, five items are required. These include three static components—Stepchamfer, chamfer insert, and trim die—and two moving components—the punch and the knockout. The punch is attached to the moving part of the press and moves vertically with a stroke of 3.5 mm and a constant velocity of 100 mm/s. Its role is to form the workpiece in conjunction with the fixed components chamfer insert and Stepchamfer, which are the most stressed tools and therefore the focus of this study. Using finite elements and varying the friction coefficient, the stresses of these two components have been calculated. The knockout, which applies a constant force of 100 kN in the opposite direction to the punch movement, is responsible for clamping the part during the forming process.

The objective of the simulation is to determine the stress levels experienced by the chamfer insert and Stepchamfer dies. The first simulation employs a friction coefficient of 0.3, which represents the friction between two steels lubricated with standard cutting oil and is considered representative of the actual process. This value was used in other works [27,28]. Subsequently, a second simulation is conducted with a friction coefficient of 0.1, with the assumption that this modification will result in lower stress levels on both

dies. The simulation model, as shown in Figures 2–4, features fixed dies and a punch stroke of 3.5 mm.

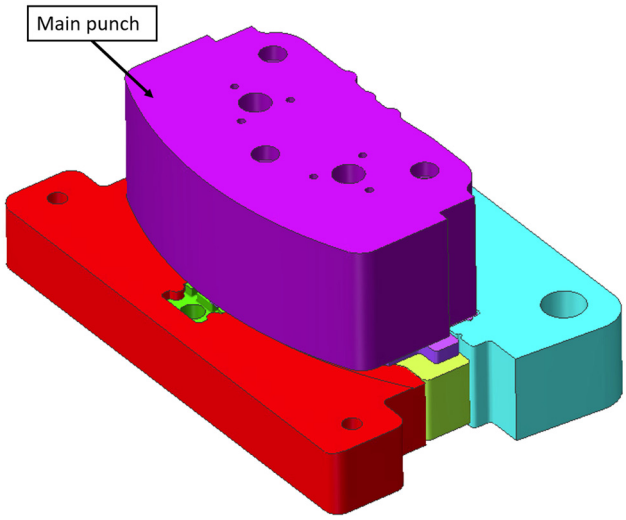

Figure 2. Simulation model.

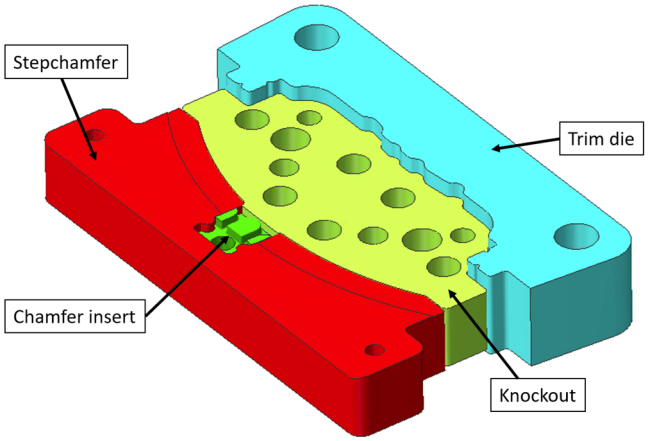

Figure 3. Bottom part of the simulation model.

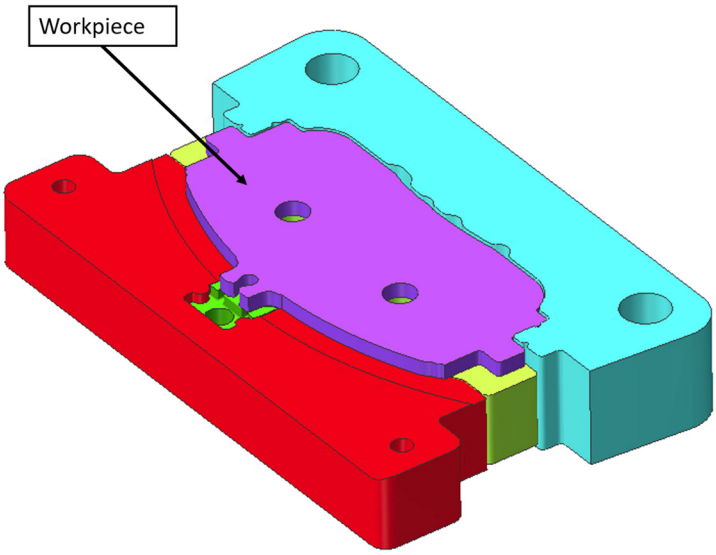

Figure 4. Workpiece.

The part's design considers the previous process steps that define the contour and holes in earlier stages of the die. It is crucial to leave sufficient material for the forming process. The part has a thickness of 6 mm.

2.2. Simulation Parameters

The simulations are performed using the software Simufact Forming 15.0 (v 15.0, Hexagon, Hamburg, Germany). Different calculation strategies are utilized, using the finite element method for the tooling stress and finite volume method for the part forming. The FV mesh, also referred to as the volume mesh, comprises Eulerian elements that remain stationary and do not undergo deformation or displacement. Their primary function is to calculate and depict the flow of material. Furthermore, the FV solver is built upon the explicit MSC Dytran solver. Initially, in the part forming simulation, 87,800 elements are created Figure 5, a quantity that increases to 114,400 due to a consecutive remeshing. Over the course of these simulations, the matrix's constituents are confined to limited movement across all axes, with the exception of the knockout that possesses mobility exclusively in the z-axis and imposes a retention force as previously expounded. Furthermore, these components are treated as rigid elements in the simulation. Both simulations have the same characteristics except for the friction coefficients. For friction, the Shear model is utilized, and different coefficients are defined for each simulation (0.1 and 0.3). Because of the cold forming, the influence of temperature is discarded. For the finite volume meshing, a size of 0.75 mm is used for each element and all dies have been defined as rigid. A surface mesh is employed with triangles as elements. The minimum element size is 0.2 mm. Furthermore, 100° is defined for the vertex angle and 60° for the edge angle. In addition, level 3 refinement boxes have been included in the area where plastic deformation is performed. Parameters have also been defined to launch the remeshing process. This remeshing is executed every 7% of the total stroke of the upper die, and if any element edge length is deformed twice its initial size. Parallel computing with four cores (parallelization) is used. The option of expensive check contact 3D to improve the accuracy of the simulation and a Taylor-type adaptive step control to increase the computational increments when complex contacts appear are used. The results are obtained every 0.25 mm.

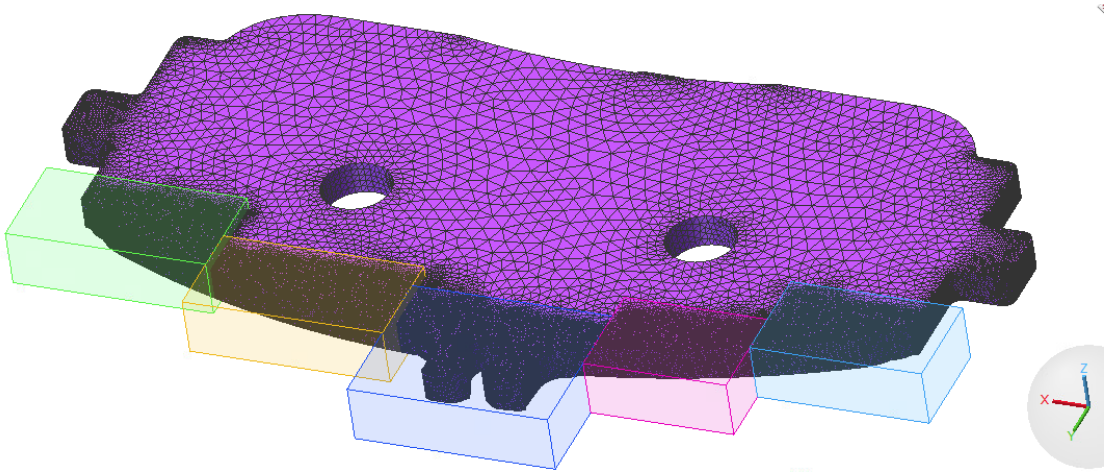

Figure 5. Meshing of the part.

Considering the results of the previous simulations, finite element simulations of the parts are performed using two friction coefficients. In these simulations, the pressures that the material applies on these parts are imported as a boundary condition. The restriction of movements is placed by a constraint plane. A mesh is made with four nodes tetrahedron-type elements and a global size of 2.5 mm. In addition, the element size in critical areas is reduced to 0.1 mm using local refinement boxes and adding the condition of increasing the number of elements in areas of small curvature. The numbers of elements in the parts are about 475,000 and 490,000. A material of the software library called Rigid (Young's

modulus of 210 GPa and yield strength of 20,000 MPa) is assigned to calculate the Von Mises stresses. Multifrontal Sparse is used as the solver, and the simulation is calculated for six specific increments of the forming process, including the end of stroke. Both tools are constrained with the plane on the base, and the contact is defined as the glued type.

2.3. Modeling Materials' Properties

An important parameter for the FE simulation is the flow curve of the material. The steel used in this stamping process is the S235JR Table 1. It is a structural steel commonly utilized in the industry and is known for its versatility. In this case, the thickness defined for the study is 6 mm sheet steel.

Table 1. Elemental composition of the S235JR, provided by the supplier.

Steel	C (%)	Mn (%)	Si (%)	P (%)	S (%)
S235JR	0.078	0.782	0.013	0.013	0.007

A compression test is effectuated to determine the stress/strain behavior of the S235JR [29]. The tensile test is usually chosen to obtain the material properties, but in this case, it is discarded. The tensile test only gives accurate results until necking, whereas the compression test obtains precise results during a longer run of the trial. There are five tests performed to ensure the results' reliability. A universal test machine (MicroTest EM2/200/FR) is used to obtain the flow curve of the steel. The equipment consists of two flat grinded parallel platforms: one is fixed and the other is movable. This equipment captures the force needed in each position (every 0.025 s) of the stroke (10 mm), maintaining a constant velocity of 100 mm/min.

The specimens are cylindrical Ø8 × 16 mm and are compressed by 10 mm (final height 6 mm) Figure 6. Contacts between the specimen and platforms are lubricated with PTFE spray to reduce the influence of friction as much as possible. Then, the results are obtained and transformed according to the assumption of the material volume invariability [30]. First, engineering stress and strain are calculated.

Figure 6. Specimen before and after the test.

The FE simulation needs a material flow curve to model deformation during the forming process, in particular, the plastic region of the curve. The collected data from the compression experiment are insufficient. This is because the end of the curve is discarded, eliminating the effect of friction. Consequently, the curve must be extrapolated for finite element computations. This way, the FE simulation can run using the same material properties obtained in the experimental test.

As is well known, there are many mathematical functions to model the curve [31,32]. Some of the most used are Hollomon [33] and Voce [34], expressions (1) and (2), respectively.

$$\sigma_H = k \cdot \varepsilon^n \quad (1)$$

$$\sigma_V = B - (B - A) \cdot e^{m \cdot \epsilon} \quad (2)$$

To find a suitable adjustment among the experimental curve and the mathematical, both models are studied [2]. The values of "k" and "n" from Hollomon's model are analyzed for each compression test. It is calculated by the least squares fit among the true stress–strain plastic region. Additionally, test number two is discarded because of its deviation from the other results. Table 2 shows the values of each test and the corresponding average value and standard deviation.

Table 2. Hollomon model's results for "k" and "n".

Test Number	n	k
Test 1	0.18	763.78
Test 2	0.11	701.56
Test 3	0.16	730.87
Test 4	0.15	722.15
Test 5	0.18	705.33
$\overline{X}$	0.16	724.74
Σ	0.03	24.91

A similar procedure is followed to calculate Voce's model [35]. Equation (2) is derived with respect to strain, and least squares are applied in order to obtain the values of "m" and "B". Finally, the value "A" is calculated by applying a natural logarithm on both sides of the derived equation and least squares are used again. Table 3 shows the results of each test. Furthermore, the results of test number five are discarded.

Table 3. Voce model's results for "m", "B", and "A".

Test Number	m	B	A
Test 1	−10.04	659.44	416.78
Test 2	−11.14	661.04	413.78
Test 3	−11.90	650.65	445.39
Test 4	−10.22	654.20	429.08
Test 5	−8.38	624.06	275.33
$\overline{X}$	−10.34	649.88	396.07
σ	1.34	15.02	68.63

Both models fit properly with the experimental curve shown in Figures 7 and 8. However, Voce's model is selected due to a higher level of coincidence with the experimental data.

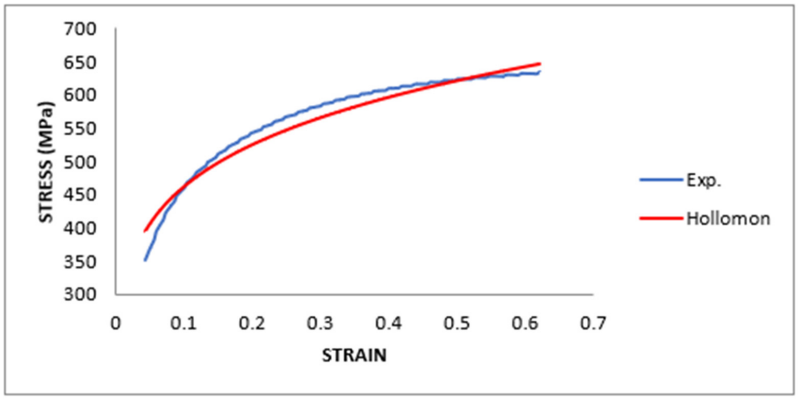

Figure 7. Comparison between Hollomon and experimental stress–strain curve.

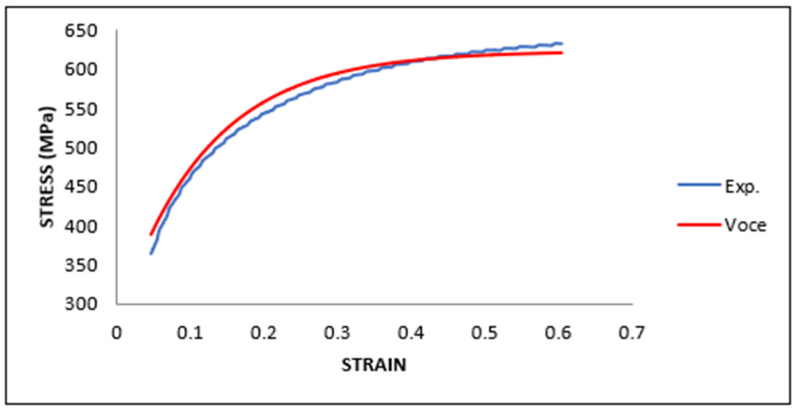

Figure 8. Comparison between Voce and experimental stress–strain curve.

2.4. DLC Coatings

On the side of the field tests, a surface treatment is applied to the tool. The objective of this is to reduce the friction coefficient of tools in order to validate the results obtained in the simulations. A PVD (physical vapor deposition) coating is applied, more specifically a DLC coating. DLC (diamond-like carbon) coatings have been recognized as valuable coatings in recent years due to their wear behavior, low friction coefficient, and high hardness or inert behavior, among others. All of these characteristics make them an ideal candidate for tribological and anticorrosive applications. On the other hand, the residual stresses generated when applying DLC to the substrate cause the coating–substrate adhesion to not be as good as it should be. However, this issue has been significantly reduced by the HIPIMS technique and the innovative application of positive pulses in the unloading phase [26].

The depositions are carried out by Magnetron Sputtering with a pumping rate of 600 L/s and equipped with rectangular magnetrons (HS100400) from Gencoa. Graphite (99.95% C) and WC:Co (6% Co) (both with an area of 400 cm^2) and a circular Cr target (area of 20 cm^2) are used as the targets. During the coating deposition, the substrates are placed at distances of 10 cm from the Cr target and 13 cm from the WC:C and graphite target. The vacuum pressure is maintained at 10–4 Pa, while the argon working pressure is set at 0.5 Pa.

As a pre-treatment, argon sputtering is performed on the substrates for 15 min by applying a DC voltage of −400 V with a frequency of 150 kHz. Then, a bonding layer is applied using the Cr target, with a 6 kW HiPIMS power supply and a circular magnetron at a voltage of −1000 V, with a pulse duration of 100 µs, frequency of 100 Hz, and maximum discharge density of 1.5 A/cm^2. The thickness of the Cr target is approximately 100 nm. Then, the anchor layer is applied, which acts as a bonding layer between the coating and the substrate. For this, the WC:C target is used with a voltage of −1050 V, pulse duration 2.7 µs, and a frequency of 150 kHz. The power density is 1.5 W/cm^2, achieving a layer thickness of 1.2 µm. Finally, the 6 kW Hi-PIMS power supply is connected to the graphite target for a–C application.

To perform the tribomechanical tests, a Microtest MT series equipment (Microtest S.A., Microtest S.A., Madrid, Spain) is utilized. Pin-on-disk tests are conducted with 6 mm alumina balls serving as pins. These balls have a surface maximum roughness of Ra_{max} = 0.050 µm and a hardness of about 1650 HV. The coated tool steels are used as disks. The tests are performed under a 40 N load, 200 rpm, and 20,000 cycles, generating a Hertzian contact stress of 2.6 GPa. The tests are repeated three times at 8, 10, and 12 mm (track radii). The tool steels and coatings used in this study have excellent tribological properties, so a high load and sufficient revolutions are necessary to produce a measurable and homogeneous wear track. These testing conditions are more similar to actual industrial applications such as cold stamping or forming, where high pressure is applied. The experimental results are shown in Figures 9 and 10. As expected, the samples coated with DLC layers show values around 0.10. The results of the friction coefficient are lower than

those reported in Reference [36], where the friction coefficient of the nitrogen-doped DLC coating increased steadily and finally reached a value of 0.2, whereas that for the DLC sample reached a value of 0.3 at the end of the test. However, the friction coefficients are very similar to those reported in Reference [37].

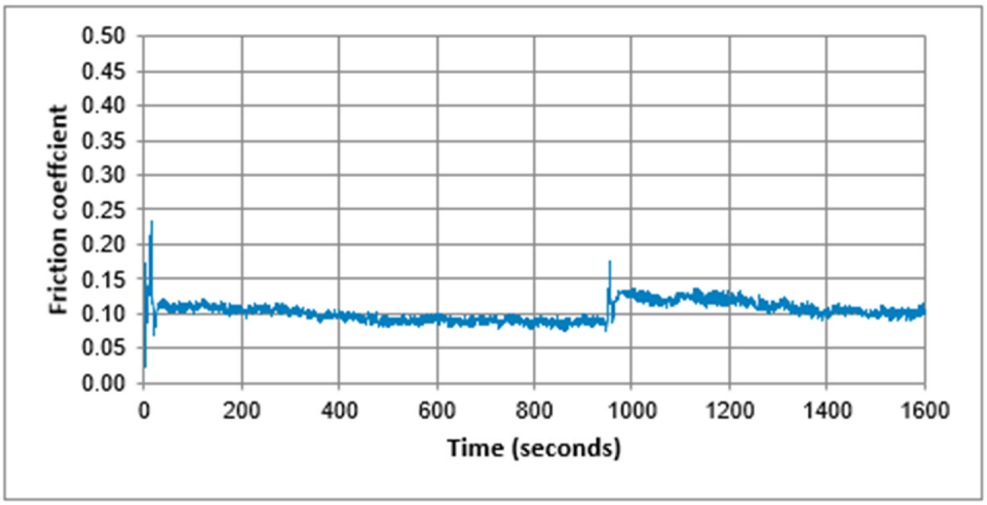

Figure 9. Friction coefficient of the coated parts R12.

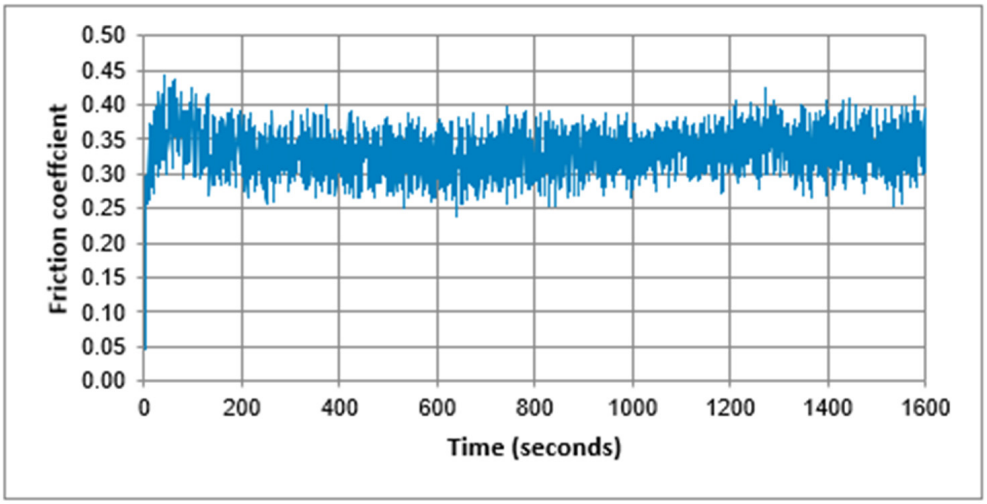

Figure 10. Friction coefficient of the uncoated parts R12.

3. Results

3.1. Plastic Strain

In this section, the deformation process of the part is analyzed. The chamfer insert forms the central area of the part. The Stepchamfer, on the other hand, is the one which facilitates the deformation on both sides by making a kind of step. Figure 11 shows the deformation of the part when the deformation coefficient is 0.3. Figure 12 shows the deformation of the part when the friction coefficient is 0.1. It could be considered that both deformations are practically the same. There are some small differences, but in general terms, the parts deform in the same way. Therefore, in this work, it is assumed that the change of the friction coefficient does not significantly affect the deformation of the part.

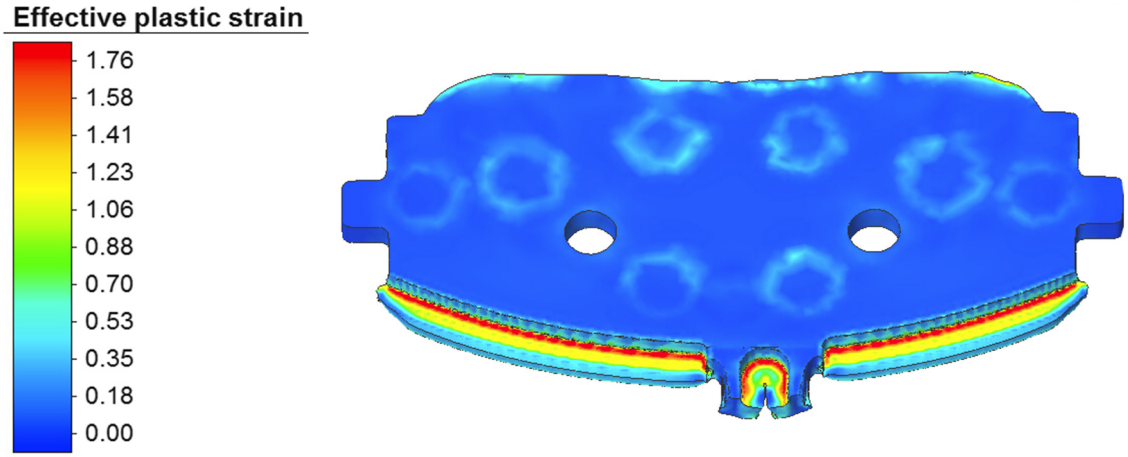

Figure 11. Effective plastic strain of the part corresponding to the simulation with friction coefficient of 0.3.

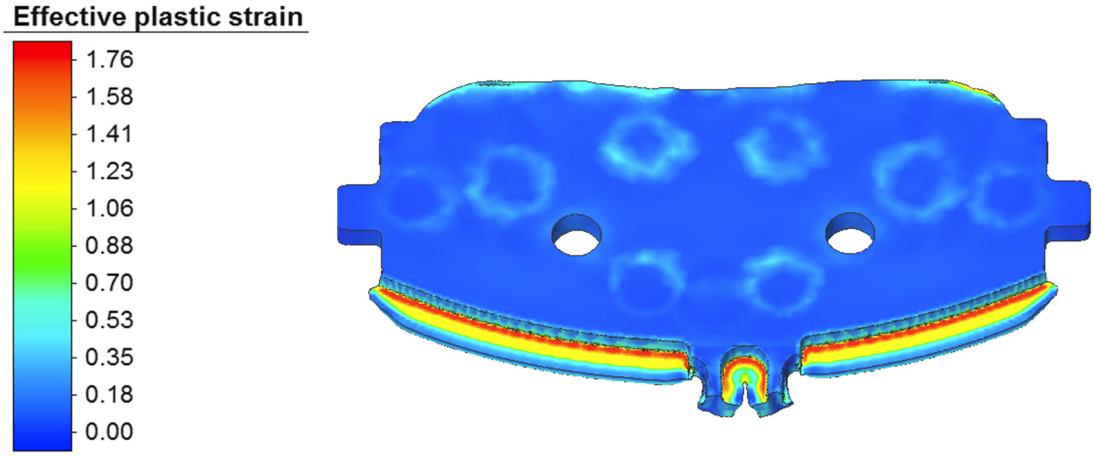

Figure 12. Effective plastic strain of the part corresponding to the simulation with friction coefficient of 0.1.

3.2. Die Stress

In this section, the stresses suffered by the selected tools are studied. For this purpose, the Von Mises stress is utilized.

The images below demonstrate the impact of the forming process on the Stepchamfer. The (a) image represents the tool with a friction coefficient of 0.3, while the (b) image shows the coated tool (with a friction coefficient of 0.1). There are no red areas in either image, which indicate that there are no critical zones. Despite the mechanical strength of the steel being 2550 MPa, areas with stress levels above 2000 MPa are identified as conflictive. The pictures illustrate that when reducing the friction coefficient, the stress also decreases. In Figure 13b, which represents the tool with a coefficient of 0.1, the color intensity is significantly reduced, indicating lower stress requirements. It can be stated that the tool which has been coated has not exceeded the threshold of 1500 MPa, which implies that its strength or durability has remained within the expected limits. On the other hand, the uncoated version of the same tool has been subjected to a stress level of 1800 MPa, which is higher than that of its coated counterpart. This difference in stress levels suggests that the coating has had a positive effect on the tool's ability to withstand external forces and has helped to prevent its failure or breakdown under high pressure.

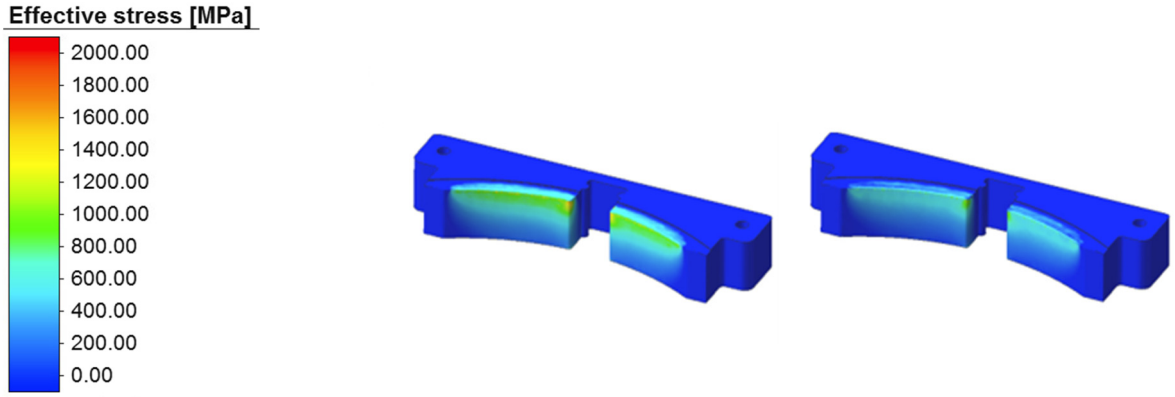

(**a**) (**b**)

Figure 13. Von Mises stress on Stepchamfer. (**a**) Simulation with a friction coefficient of 0.3. (**b**) Simulation with a friction coefficient of 0.1.

Figure 14 corresponds to the stresses received in the chamfer insert. As in the previous case, a reduction in stress can be seen when the tool has a friction coefficient of 0.1. In addition, the 0.3 and 0.1 friction coefficients show red areas. This means that these areas are above the critical range of the material and are therefore subject to possible failures. Hence, these are areas where failures or ruptures could appear in the field tests. However, by reducing the coefficient to 0.1, there is also a significant reduction of the conflict zone. As was observed in the previous case, the tool which is equipped with a coating has undergone a noteworthy decrease in its stress levels. This implies that the coating has had a positive impact on the tool's ability to withstand external pressure and has effectively mitigated the damaging effects of stress.

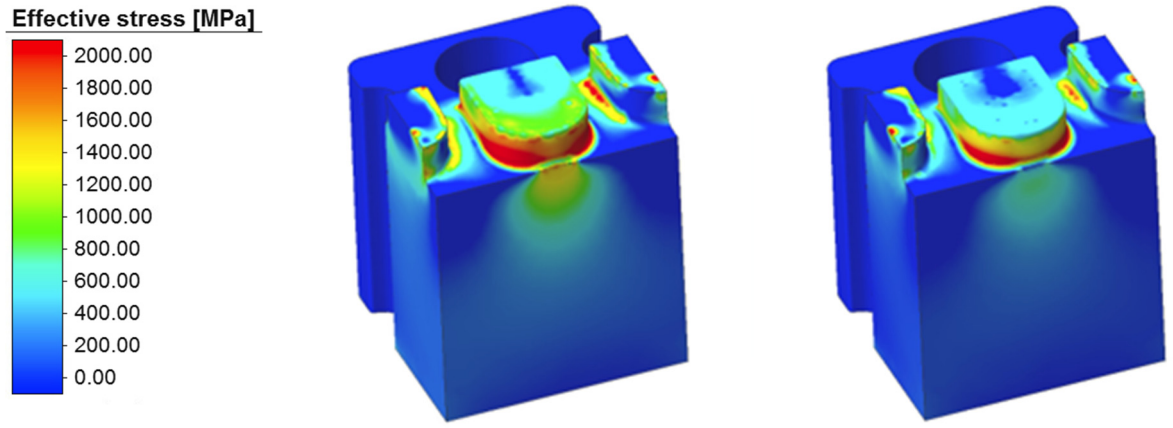

(**a**) (**b**)

Figure 14. Von Mises stress on the chamfer insert. (**a**) Simulation with a friction coefficient of 0.3. (**b**) Simulation with a friction coefficient of 0.1.

3.3. Die Load

In this section, the die loads of the chamfer insert and Stepchamfer are analyzed. Figure 15 shows that the tool Stepchamfer with a friction coefficient of 0.3 achieves a reaction force of 980 kN. The same tool with a friction coefficient of 0.1 obtains 800 kN. This means that when reducing the friction coefficient of the tool Stepchamfer from 0.3 to 0.1, the tonnage is reduced by about 20%. In Figure 16, the force of the chamfer insert can be seen. This tool with a friction coefficient of 0.3 obtains 180 kN. If we reduce the friction coefficient on the same tool to 0.1, the amount of force is reduced to 145 kN. In this case, the reduction is about 20%.

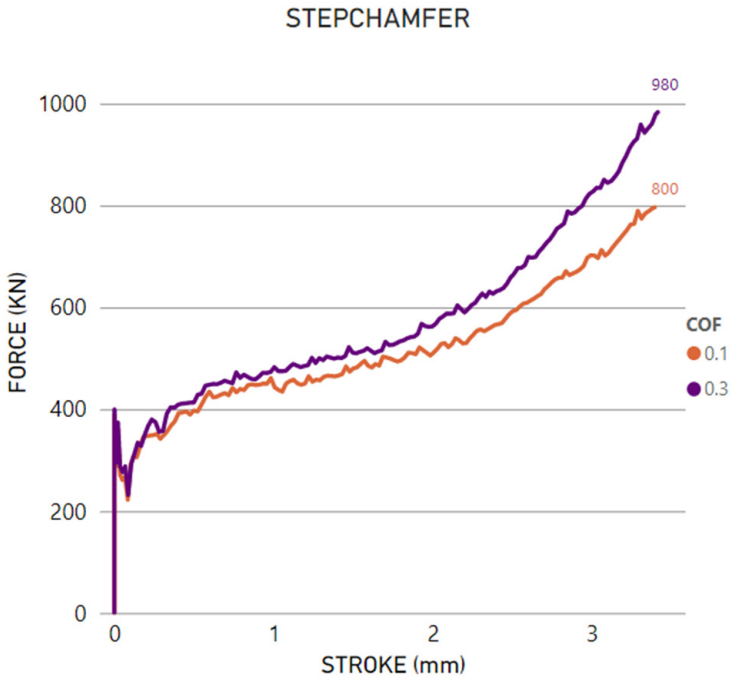

Figure 15. Die load of the tool Stepchamfer.

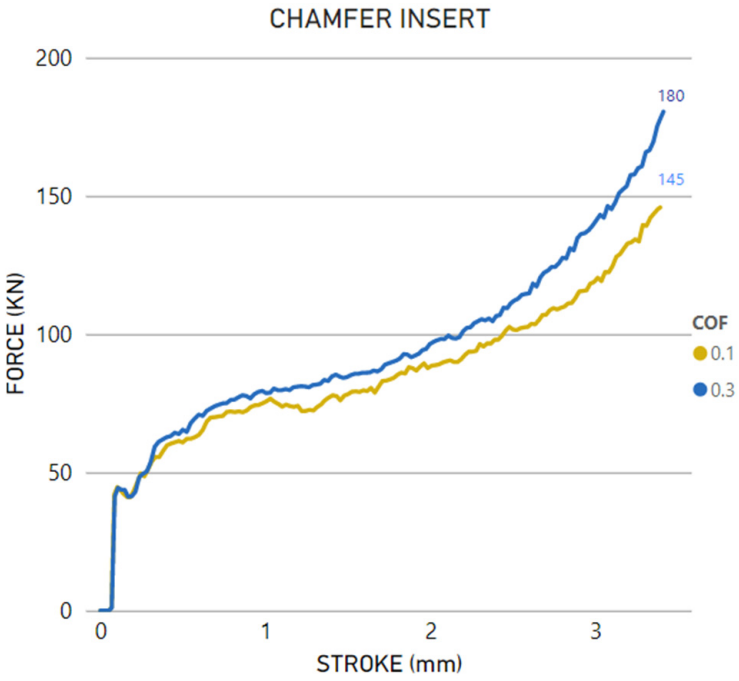

Figure 16. Die load of the chamfer insert.

The graph presented provides a clear illustration of the relationship between friction reduction and the corresponding decrease in the force required for forming a part. This is because the total force required for forming can be separated into two different components. The first is the force required to deform the material, while the second is the force required to overcome friction between the tools and the sheet metal.

Consequently, when the friction coefficient is decreased, the force required for forming is also reduced. This is because less force is needed to overcome the reduced friction, resulting in a decrease in the total force required for the forming process. By understanding this relationship between the friction reduction and force requirements for forming, it is

possible to optimize the forming process to reduce costs associated with tool wear and tear, while also improving the product quality.

3.4. Industrial Tests

In order to validate the theoretical results obtained in the finite volume simulations, field tests are carried out in a real manufacturing process. Two different tests are completed, one with the uncoated tool (friction coefficient of 0.3) and the other with a coated tool (friction coefficient of 0.1). In both cases, the steel used is a tool steel 1.2379. This is a high-carbon, high-chromium steel that is widely used in the production of cutting tools, dies, and molds. It is also known by the names AISI D2 steel or DIN 1.2379 steel Table 4. This steel has a high level of wear resistance, toughness, and compressive strength, which makes it suitable for applications that require high durability and reliability. It has excellent resistance to abrasion, chipping, and deformation at high temperatures, making it ideal for use in cold work applications.

Table 4. Elemental composition of the 1.2379, provided by the supplier.

Steel	C (%)	Cr (%)	Mo (%)	Mn (%)	Si (%)
1.2379	1.51	11.46	0.73	0.38	0.47

The experiments are conducted in a 600-ton PATEC press. These tests have made it possible to study the consequences of reducing the friction coefficient in tools. Whether or not the final geometry of the part changes significantly is analyzed.

The deformation suffered by the part is practically the same as in the models obtained by simulation. In addition, a small geometrical deviation is found among the parts produced by the coefficient 0.3 (Figure 17) and the part produced by the coefficient 0.1 (Figure 18). However, those differences could be discarded because they are irrelevant, and in general terms, all models are similar. Consequently, the influence of friction in the part could be ignored. This portion is considered scrap in subsequent processes, and these variations can be ignored. Consequently, the modification does not have any impact on the stamping production process.

Figure 17. Final geometry of the part corresponding to the field test with a friction coefficient of 0.3.

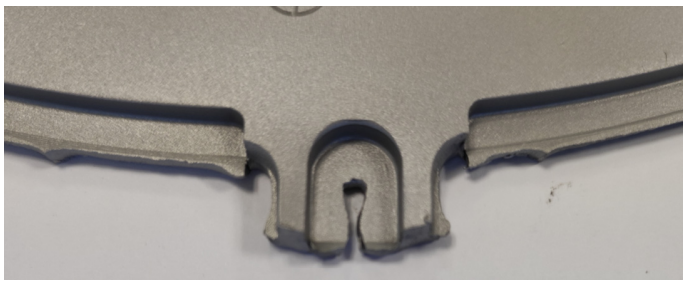

Figure 18. Final geometry of the part corresponding to the field test with a friction coefficient of 0.1.

Additionally, the service life of tools has been studied, considering factors such as wear or failures. To continue with the study, the tools are tested after 65,000 cycles. On the one hand, there are the tools with a coefficient of 0.3, and on the other, there are those with a coefficient of 0.1. By analyzing the tool Stepchamfer Figure 19, it could be seen that neither of the two versions (0.3 and 0.1) has suffered any failure. This is in concordance with the Von Mises stresses studied in the finite element simulations, where there was no area in red with values above the yield strength of the steel. In addition, wear marks can be seen on both tools. However, neither of them has suffered major wear. In the coated version, traces could be seen which indicate that the coating has disappeared on the edge.

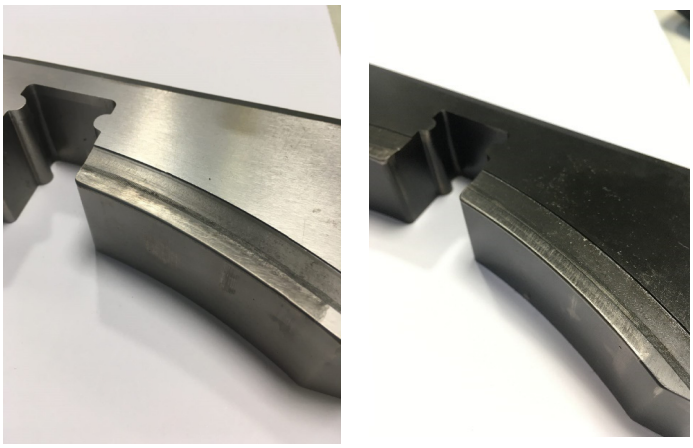

(**a**) (**b**)

Figure 19. Tool Stepchamfer after 65,000 cycles, (**a**) coefficient 0.3, (**b**) DLC coating applied, and coefficient 0.1.

The chamfer insert, Figure 20, with a coefficient of 0.3 has suffered irreparable damage. The rear part of the tool has been damaged and the tool has become unusable. Regarding the simulations, red areas could be seen on the chamfer insert, which are susceptible to possible failures. Moreover, the field test has confirmed these results. However, it is certainly clear from the simulations that there is another area with a higher probability of failure. The version with a coefficient of 0.1 is not damaged and is able to continue working. Finally, it should be mentioned that wear marks are found in both versions.

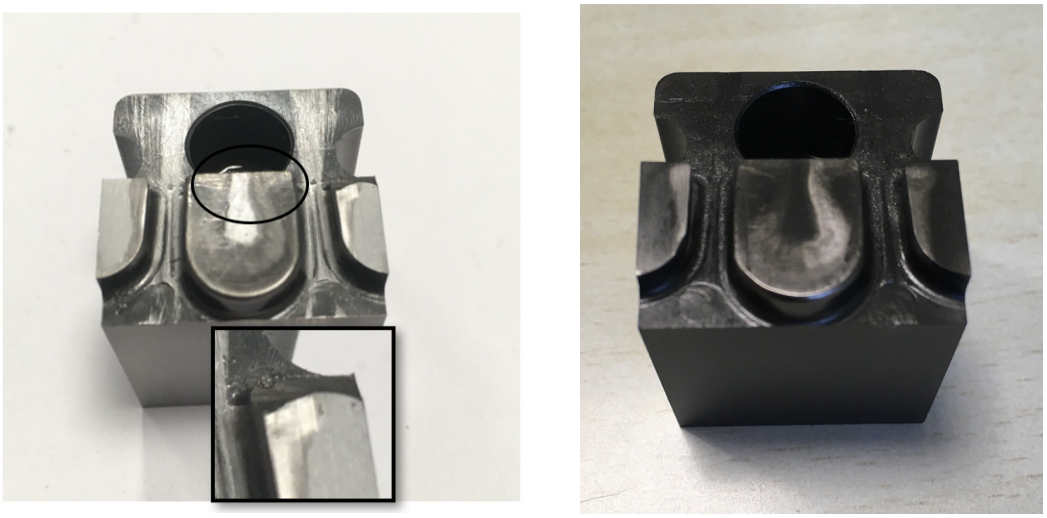

(**a**) (**b**)

Figure 20. The chamfer insert after 65,000 cycles, (**a**) coefficient 0.3, (**b**) DLC coating applied, and coefficient 0.1.

In the direction of quantifying the wear of each tool in the industrial test, the roughness of each tool has been studied. The study is carried out using a confocal microscope and advanced analysis software (SENSOMAP). The value of the arithmetic mean deviation of the roughness profile (Sa) is obtained for each tool before and after working (65,000 cycles). This is a parameter commonly used to quantify the surface roughness of a material or component, particularly in engineering and manufacturing industries.

Tables 5 and 6 show the results of roughness (Sa) obtained using the confocal microscope. The tools have obtained higher Sa values after 65,000 cycles, and roughness has increased after the tools work. Figure 21 shows the behavior of each tool depending on the friction coefficient. Tools with a friction coefficient of 0.3 have increased their Sa by 0.5 µm. The coated tools with a friction coefficient of 0.1 have increased their Sa by 0.25 µm.

Table 5. Sa (µm) values for the tool Stepchamfer, before and after working (65,000 cycles).

Friction Coefficient	0 Cycles	65,000 Cycles
0.3	0.71 ± 0.03	1.20 ± 0.29
0.1	0.52 ± 0.05	0.74 ± 0.12

Table 6. Sa (µm) values for the chamfer insert, before and after working (65,000 cycles).

Friction Coefficient	0 Cycles	65,000 Cycles
0.3	0.38 ± 0.05	0.86 ± 0.29
0.1	0.39 ± 0.05	0.64 ± 0.12

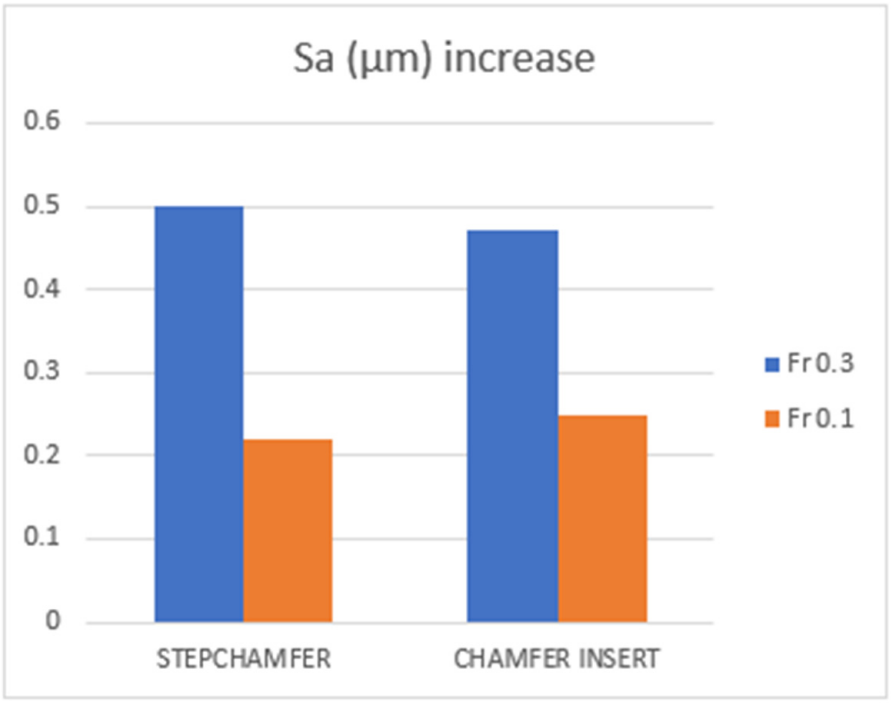

Figure 21. Increment of Sa (µm) after 65,000 cycles for each tool and friction coefficient.

Figure 22 shows the points where the confocal analysis is conducted. The following figures (Figures 23–26) show the confocal microscope images of the different tools with each friction coefficient before and after 65,000 cycles. In image (a), the grooves made by the grinding machine can be seen, either in the coated tools or in the uncoated ones. This indicates that the coating copies the surface below it. In image (b), it can be seen how after 65,000 cycles, the initial surface is altered depending on the flow of the material in the forming operation.

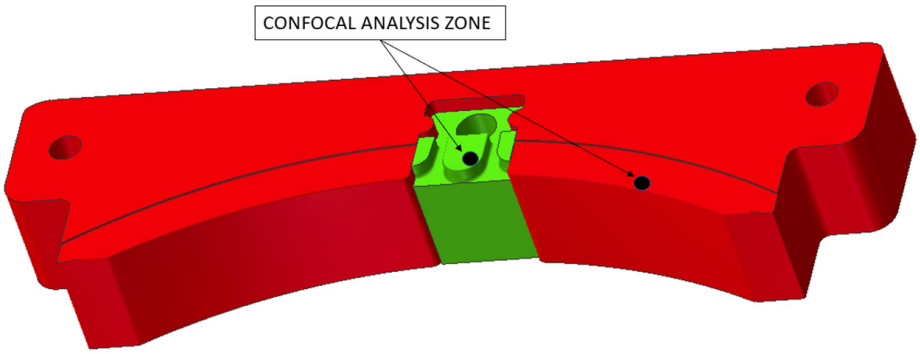

Figure 22. Points under confocal microscope analysis.

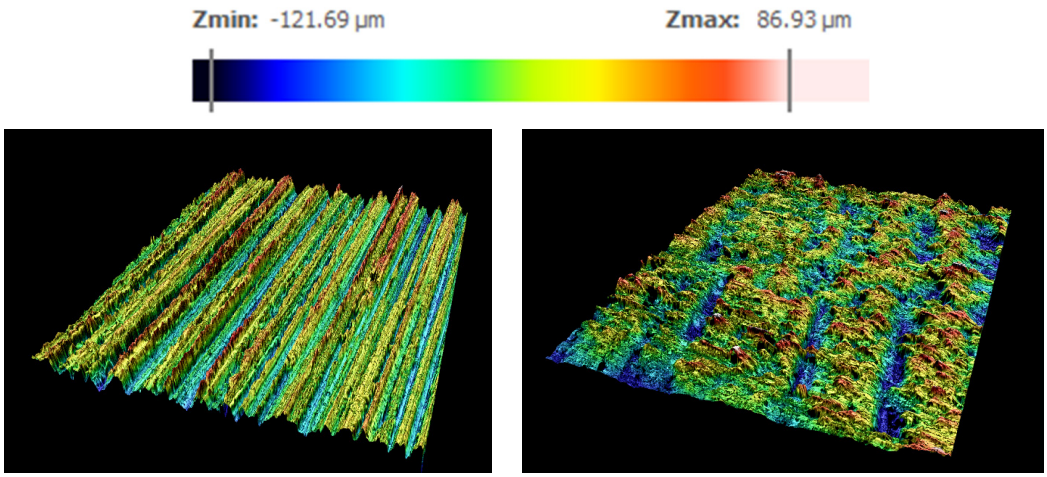

Figure 23. Sensomap image of the Stepchamfer with 0.3 friction coefficient (**a**) before working Sa 0.68 µm; (**b**) after 65,000 cycles, Sa 0.99 µm.

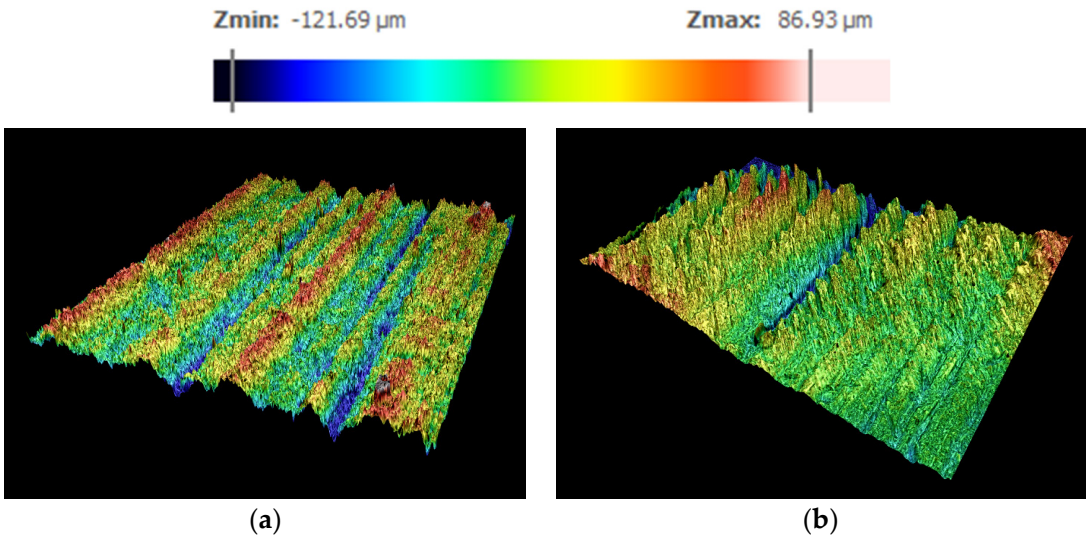

Figure 24. Chamfer insert with 0.3 friction coefficient, Sensomap images (**a**) before working Sa 0.33 µm; (**b**) after 65,000 cycles, Sa 0.95 µm.

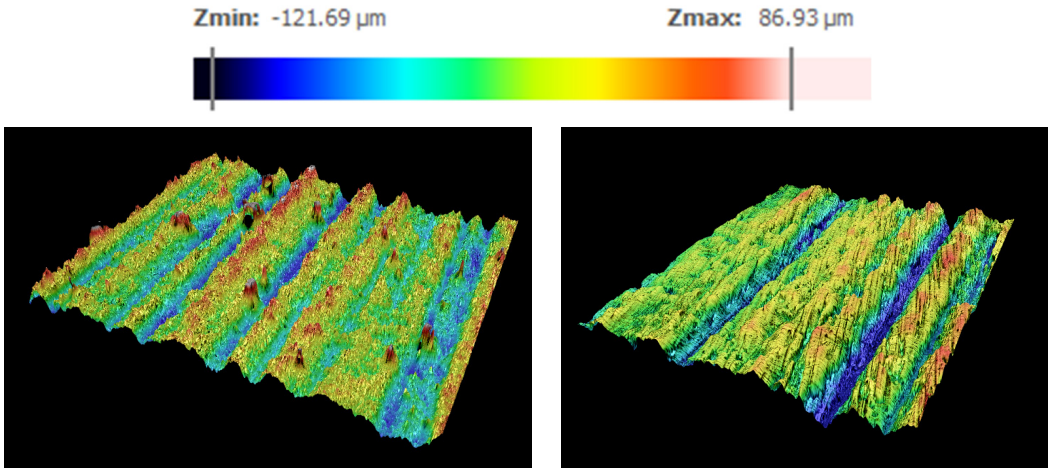

Figure 25. Sensomap image of tool Stepchamfer with 0.1 friction coefficient (**a**) before working Sa 0.48 µm; (**b**) after 65,000 cycles, Sa 0.73 µm.

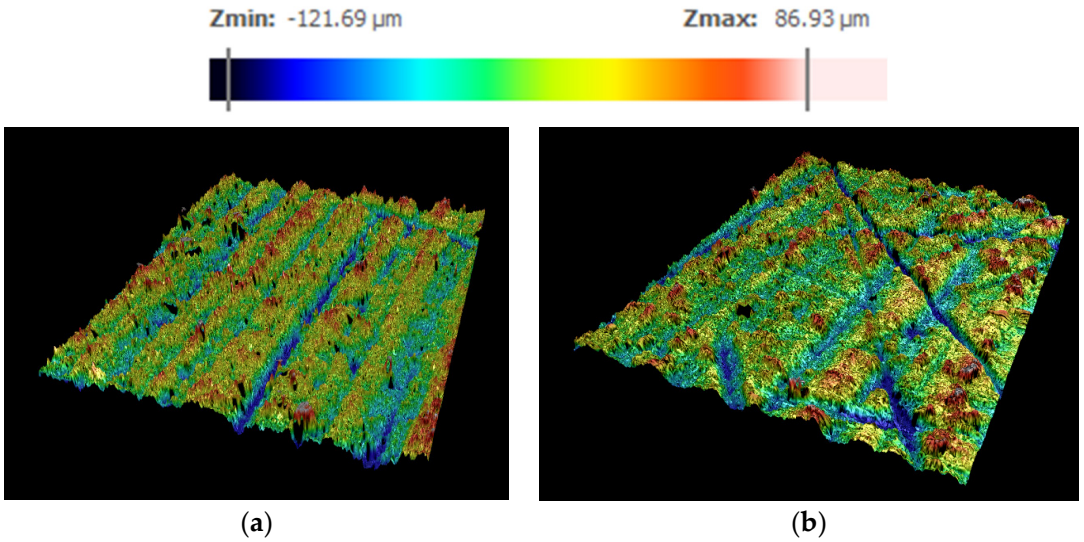

Figure 26. The chamfer insert with 0.1 friction coefficient, Sensomap images (**a**) before working Sa 0.34 µm; (**b**) after 65,000 cycles, Sa 0.60 µm.

This paragraph points out an important issue that has not been discussed, which is the generation of grooves during the tool finishing process. When tools are manufactured using machining processes, they typically undergo a finishing process that results in the creation of grooves. These grooves are formed in a particular direction, and it is critical that they are aligned with the direction of material flow. This alignment is important because it facilitates the forming process and improves the overall quality of the final product.

The generation of grooves in the tool finishing process is a common occurrence, and it is typically caused by the cutting action of the machining tool. The direction of these grooves is determined by the direction in which the tool is moved along the surface of the material. It is essential that these grooves are aligned with the direction of material flow because they play a crucial role in facilitating the forming process. If the grooves are not aligned with the material flow direction, they can impede the flow of material and cause defects in the final product.

4. Conclusions

This section discusses the article's conclusions regarding the impact of reducing the friction coefficient on tool performance. By reducing the coefficient of friction, the stresses on tools can be minimized, which can lead to a longer tool life. This effect can be observed in two ways: it can help in preventing total tool breakage, and it also reduces tool wear. While the reduction of the friction coefficient can also impact the formation of the final part, this is not a significant concern in this context.

- Finite volume simulations demonstrate that changing the friction coefficient directly affects the stresses suffered by tools. When the friction coefficient is reduced, the stress is also reduced by 20%.
- Changing the friction coefficient of the tools does not affect the forming of the part. The differences between the two parts, even if there are any, are practically minimum. In both the simulations and field tests, the differences are practically non-existent.
- Confocal analyses are suitable tests to study the grooves left by the grinding machine. Therefore, the direction in which the parts are ground is very relevant and directly affects how the material flows. In addition, it could also be seen how the material is able to deform these grooves.
- The tool Stepchamfer has not suffered any remarkable damage, and this is in line with the calculations made in the simulations. There are no stresses exceeding the elastic limit of the material. The tool with coating achieves a maximum stress level of 1500 MPa, whereas the uncoated tool reaches 1800 MPa.
- The chamfer insert with the friction coefficient of 0.3 has a fracture on the back side. This is in accordance with the simulations. However, it is certainly clear from the simulations that there is another area with a higher probability of failure. This area is where three different vertices meet and may be a conflict point. However, another type of failure cannot be dismissed.
- In both tools, wear has been higher when the friction coefficient is 0.3. Sa values have been increased approximately 0.5 μm.

Author Contributions: Conceptualization, R.L. and J.A.G.; methodology, A.C.; software, D.S.; validation, E.B.; formal analysis, A.C.; writing—original draft, E.B.; writing—review and editing, E.B.; visualization, D.S. All authors have read and agreed to the published version of the manuscript.

Funding: This research was funded by the Government of Navarre grant number 0011-1408-2020-000024.

Data Availability Statement: For more information https://www.nuadi.com/contact/.

Acknowledgments: We would like to express our gratitude to the Government of Navarre for their financial assistance with a part of this study.

Conflicts of Interest: The authors declare no conflict of interest.

References

1. Hashim, S. *Comprehensive Materials Processing*; Elsevier: Amsterdam, The Netherlands, 2014. [CrossRef]
2. Gram, M.; Wagoner, R. Fineblanking of high strength steels: Control of material properties for tool life. *J. Mater. Process. Technol.* **2011**, *211*, 717–728. [CrossRef]
3. Baer, O.; Feuerhack, A.; Voigts, H.; Bergs, T. Investigation of the Mechanical Punch Loads during Fine Blanking of High-Strength Steels with Cemented Carbide. *Procedia Manuf.* **2019**, *34*, 90–100. [CrossRef]
4. Tang, B.; Liu, Y.; Mao, H. Investigation of a novel modified die design for fine-blanking process to reduce the die-roll size. *Procedia Eng.* **2017**, *207*, 1546–1551. [CrossRef]
5. Thipprakmas, S.; Jin, M.; Tomokazu, K.; Katsuhiro, Y.; Murakawa, M. Prediction of Fineblanked surface characteristics using the finite element method (FEM). *J. Mater. Process. Technol.* **2008**, *198*, 391–398. [CrossRef]
6. Kwak, T.; Kim, Y.; Bae, W. Finite element analysis on the effect of die clearance on shear planes in fine blanking. *J. Mater. Process. Technol.* **2002**, *130–131*, 462–468. [CrossRef]
7. Wu, Y.; Groche, P. Influence of Tool Finishing on the Wear Development in Strip Drawing Tests with High Strength Steels. *Tribol. Online* **2020**, *15*, 170–180. [CrossRef]

8. Groche, P.; Moeller, N.; Hoffmann, H.; Suh, J. Influence of gliding speed and contact pressure on the wear of forming tools. *Wear* **2011**, *271*, 2570–2578. [CrossRef]
9. Bayer, R.; Sirico, J. The influence of surface roughness on wear. *Wear* **1975**, *35*, 251–260. [CrossRef]
10. Groche, P.; Christiany, M.; Wu, Y. Load-dependent wear in sheet metal forming. *Wear* **2019**, *422–423*, 252–260. [CrossRef]
11. Podgornik, B.; Hogmark, S. Surface modification to improve friction and galling properties of forming tools. *J. Mater. Process. Technol.* **2006**, *174*, 334–341. [CrossRef]
12. Sorgente, D.; Lombardi, A.; Coviello, D.; Scintilla, L.; Fontana, M. A strain-dependent model for the coefficient of friction in the tool-blank interaction in superplastic forming. *J. Manuf. Process.* **2021**, *73*, 791–798. [CrossRef]
13. Brathikan, V.; Sangeethkumar, B.; Nitheeshwar, R.; Scidarth, K. Variation of force due to co-efficient of friction & blank diameter in deep drawing. *Mater. Today: Proc.* **2022**, *68*, 2189–2194. [CrossRef]
14. Nielsen, C.V.; Bay, N. Overview of friction modelling in metal forming processes. *Procedia Eng.* **2017**, *207*, 2257–2262. [CrossRef]
15. Tzou, G. Theoretical study on the cold sandwich sheet rolling considering Coulomb friction. *J. Mater. Process. Technol.* **2001**, *114*, 41–50. [CrossRef]
16. Zhang, D.-W.; Ou, H. Relationship between friction parameters in a Coulomb–Tresca friction model for bulk metal forming. *Tribol. Int.* **2016**, *95*, 13–18. [CrossRef]
17. Zhang, D.-W.; Xu, F.-F.; Yu, Z.-C.; Lu, K.-Y.; Zheng, Z.-B.; Zhao, S.-D. Coulomb, Tresca and Coulomb-Tresca friction models used in analytical analysis for rolling process of external spline. *J. Mater. Process. Technol.* **2021**, *292*, 117059. [CrossRef]
18. Kechidi, S.; Iuorio, O. Investigation of the effect of modular construction details on the lateral behaviour of cold-formed steel framed shear walls. *Eng. Struct.* **2022**, *268*, 114707. [CrossRef]
19. Seok, S.; Lee, J.; Choi, C.-S. A computational modeling approach for cold-formed steel bolted connections exhibiting bolt slip and bearing behavior. *Structures* **2023**, *53*, 460–473. [CrossRef]
20. Sulaiman, M.; Farahana, R.; Bienk, K.; Nielsen, C.V.; Bay, N. Effects of DLC/TiAlN-coated die on friction and wear in sheet-metal forming under dry and oil-lubricated conditions: Experimental and numerical studies. *Wear* **2019**, *438–439*, 203040. [CrossRef]
21. Claver, A.; Jiménez-Piqué, E.; Palacio, J.F.; Almandoz, E.; Fernández de Ara, J.F.; Fernández, I.; Santiago, J.A.; Barba, E.; García, J.A. Comparative Study of Tribomechanical Properties of HiPIMS with Positive Pulses DLC Coatings on Different Tools Steels. *Coatings* **2021**, *11*, 28. [CrossRef]
22. García, J.A.; Rivero, P.J.; Barba, E.; Fernández, I.; Santiago, J.A.; Palacio, J.F.; Fuente, G.G.; Rodríguez, R.J. A Comparative Study in the Tribological Behavior of DLC Coatings Deposited by HiPIMS Technology with Positive Pulses. *Metals* **2020**, *10*, 174. [CrossRef]
23. Münz, W.-D.; Schenkel, M.; Kunkel, S.; Paulitsch, J.; Bewilogua, K. Industrial applications of HIPIMS. *J. Phys. Conf. Ser.* **2008**, *100*, 082001. [CrossRef]
24. Wang, L.; Jin, J.; Zhu, C.; Li, G.; Kuang, X.; Huang, K. Effects of HiPIMS pulse-length on plasma discharge and on the properties of WC-DLC coatings. *Appl. Surf. Sci.* **2019**, *487*, 526–538. [CrossRef]
25. Hiratsuka, M.; Azuma, A.; Nakamori, H.; Kogo, Y.; Yukimura, K. Extraordinary deposition rate of diamond-like carbon film using HIPIMS technology. *Surf. Coat. Technol.* **2013**, *229*, 46–49. [CrossRef]
26. Santiago, J.A.; Fernández-Martínez, I.; Kozák, T.; Capek, J.; Wennberg, A.; Molina-Aldareguia, J.M.; Bellido-González, V.; González-Arrabal, R.; Monclus, M.A. The influence of positive pulses on HiPIMS deposition of hard DLC coatings. *Surf. Coat. Technol.* **2019**, *358*, 43–49. [CrossRef]
27. Salcedo, D.; Luis, C.J.; Luri, R.; Puertas, I.; León, J.; Fuertes, J.P. Design and Mechanical Properties Analysis of AA5083 Ultrafine Grained Cams. *Metals* **2017**, *7*, 116. [CrossRef]
28. Pérez, C.J.L.; Irigoyen, R.L.; Arbizu, I.P.; Pérez, D.S.; Iriarte, J.L.; Bonel, J.P.F. Analysis of Tribological Properties in Disks of AA-5754 and AA-5083 Aluminium Alloys Previously Processed by Equal Channel Angular Pressing and Isothermally Forged. *Metals* **2020**, *10*, 938. [CrossRef]
29. Wang, X.; Li, H.; Chandrashekhara, K.; Rummel, S.; Lekakh, S.; Van Aken, D.; O'malley, R. Inverse finite element modeling of the barreling effect on experimental stress-strain curve for high temperature steel compression test. *J. Mater. Process. Technol.* **2017**, *243*, 465–473. [CrossRef]
30. Martínez, A.; Miguel, V.; Coello, J.; Manjabacas, M. Determining stress distribution by tension and by compression applied to steel: Special analysis for TRIP steel sheets. *Mater. Des.* **2017**, *125*, 11–25. [CrossRef]
31. León, J.; Luis, C.J.; Fuertes, J.P.; Puertas, I.; Luri, R.; Salcedo, D. A Proposal of a Constitutive Description for Aluminium Alloys in Both Cold and Hot Working. *Metals* **2016**, *6*, 244. [CrossRef]
32. Gupta, M.K.; Singh, N.K. Modelling and simulation on deformation behaviour of Al2014-T6 alloy beyond necking. *Mater. Today: Proc.* **2020**, *44*, 4204–4208. [CrossRef]
33. Hollomon, J.H. Tensile deformation. *Trans. Metall. Soc. AIME* **1945**, *162*, 268–290.
34. Voce, E. The relationship between stress and strain for homogeneous deformation. *J. Inst. Met.* **1978**, *74*, 537–562.
35. Sainath, G.; Choudhary, B.; Christopher, J.; Samuel, E.I.; Mathew, M. Applicability of Voce equation for tensile flow and work hardening behaviour of P92 ferritic steel. *Int. J. Press. Vessel. Pip.* **2015**, *132–133*, 1–9. [CrossRef]

36. Sharifahmadian, O.; Mahboubi, F. A comparative study of microstructural and tribological properties of N-DLC/DLC double layer and single layer coatings deposited by DC-pulsed PACVD process. *Ceram. Int.* **2019**, *45*, 7736–7742. [CrossRef]
37. Wang, L.; Li, L.; Kuang, X. Effect of substrate bias on microstructure and mechanical properties of WC-DLC coatings deposited by HiPIMS. *Surf. Coat. Technol.* **2018**, *352*, 33–41. [CrossRef]